Single-frame measurement of the complete spatiotemporal intensity and phase of ultrashort laser pulses using wavelength-multiplexed digital holography

Pablo Gabolde* and Rick Trebino

Georgia Institute of Technology, 837 State Street NW, Atlanta, Georgia 30332, USA
**Corresponding author: pablo@gatech.edu*

Received October 22, 2007; revised January 30, 2008; accepted February 1, 2008;
posted February 11, 2008 (Doc. ID 88865); published April 7, 2008

We show that a simple (few-element) arrangement for wavelength-multiplexed digital holography allows the measurement of the electric field $E(x,y,t)$ of a femtosecond laser pulse on a single shot. A slightly rotated two-dimensional diffractive optical element and a variable-wavelength filter together generate multiple spectrally resolved digital holograms that are simultaneously captured in a single frame by a digital camera. An additional simultaneous measurement of the spectral phase for a spatially filtered replica of the pulse with frequency-resolved optical gating completes this three-dimensional measurement. An experimental implementation of the technique is presented and its current limitations are discussed. © 2008 Optical Society of America

OCIS codes: 090.2880, 320.7100.

1. INTRODUCTION

Femtosecond laser pulses have found many applications due to their short length, broad bandwidth, and high peak intensity. To obtain the best results, great care is taken to ensure that the shortest pulse and best mode quality are obtained, usually by a combined use of dispersion-compensation [1,2] and adaptive-optics [3] techniques. Various diagnostic methods are available to monitor the optimization of the laser output, both in terms of its temporal [4–6] and spatial [7–12] characteristics. Unfortunately, independent spatial and temporal measurements fail to capture possible spatiotemporal distortions [13–22] because diagnostic devices for measuring the temporal behavior of the pulse usually integrate over the spatial transverse coordinates, and vice versa.

To solve this problem, the complete spatiotemporal field of a laser pulse, $E(x,y,t)$, can be measured using wavelength-scanning digital holography [23]. In this method, digital holograms are captured sequentially as the wavelength of a reference laser beam is scanned across the bandwidth of the pulse under test. The spatial field at each frequency ω_k, $E(x,y;\omega_k)$, is obtained by numerical processing of the individual digital holograms in the usual manner [24], and a measurement of the spectral phase using frequency-resolved optical gating (FROG) [5] completes the measurement. All the information needed to reconstruct $E(x,y,t)$ is obtained since the temporal field can be simply calculated by an inverse Fourier transform:

$$E(x,y,t) \simeq \frac{1}{2\pi}\sum_{\omega_k} E(x,y;\omega_k)\exp(i\omega_k t)\,\delta\omega. \qquad (1)$$

However, the scan of the wavelength requires multiple frames of data to be recorded. This, in turn, requires a stable train of identical pulses. For low-intensity experiments, performed, for example, using mode-locked oscillators, this condition is usually satisfied within 1%. This requirement can be prohibitive, however, for amplified laser systems that operate at low repetition rates or that have large shot-to-shot intensity fluctuations.

To overcome this limitation, we recently introduced a device capable of measuring the complete three-dimensional spatiotemporal electric field $E(x,y,t)$ in a single shot. Instead of recording multiple digital holograms for different wavelengths sequentially in time, we record them simultaneously in a larger two-dimensional camera frame. This large digital hologram contains all the necessary information to numerically reconstruct the full three-dimensional electric field $E(x,y,t)$. For that reason, we call our technique spatially and temporally resolved intensity and phase evaluation device: full information from a single hologram (STRIPED FISH) [25].

Optical arrangements for simultaneously recording a few holograms have been introduced in the past, but these either involve numerous beam splitters or a special cavity to generate a few replicas that must all be precisely synchronized [26]. As a result, they do not scale well as the pulse becomes more complex in time (or frequency) and the number of necessary holograms increases. STRIPED FISH, on the other hand, is based on a simple concept comprising only a few optical components that readily generate a large number of spectrally resolved holograms.

In this paper, we consider STRIPED FISH in detail.

Section 2 first presents the principles of operation of STRIPED FISH; Section 3 describes the algorithm for processing experimental data; Section 4 presents the experimental setup and results; Section 5 analyzes the design parameters of STRIPED FISH; and Section 6 discusses the characteristics and limitations of the technique.

2. PRINCIPLE OF STRIPED FISH

Let us briefly recall how off-axis digital holography may be used to reconstruct the spatial electric field $E(x,y)$ of a monochromatic laser beam [11]. The signal beam (the beam to be characterized) and a reference beam (a pre-characterized beam) are crossed at a small angle α, for example, in the vertical plane. One then measures the corresponding intensity $I(x,y)$, or digital hologram, using a digital camera:

$$I(x,y) = |E_s(x,y)|^2 + |E_r(x,y)|^2 + E_s(x,y)^* E_r(x,y) \times \exp(-iky \sin\alpha) + E_s(x,y) E_r(x,y)^* \times \exp(+iky \sin\alpha). \quad (2)$$

Due to the crossing angle and the resulting spatial fringes, the last term of Eq. (2), which contains the complete spatial field of the signal beam, can be readily extracted from the measured intensity $I(x,y)$ using a well-established Fourier-filtering algorithm [24]. Assuming that the electric field of the reference beam $[E_r(x,y)]$ is known, the spatial electric field of the monochromatic signal beam $[E_s(x,y)]$ can then be obtained.

This method is extended to broadband pulses by spectrally resolving the reference and signal pulses and generating monochromatic holograms for each frequency in the pulses. If we perform the reconstruction process at different frequencies ω_k (spaced by $\delta\omega$) that satisfy the sampling theorem and cover the bandwidth of the signal and reference pulses, we obtain the electric field $E(x,y)$ for each frequency ω_k. If the spectral phase of the reference pulse is also known, it is straightforward to reconstruct the signal field in the frequency domain, which then yields the complete field in the time domain in the form of an inverse Fourier transform given by Eq. (1).

To obtain the same information, but on a single camera frame, using STRIPED FISH, we simultaneously generate multiple holograms, one for each frequency ω_k. The pulse under test is still interfered with a (coherent and time-coincident) reference pulse at a small vertical angle $\alpha \approx 0.5°$ (about the x axis), but these two pulses then pass through a diffractive optical element (DOE)—equivalent to a low-resolution two-dimensional diffraction grating—which generates a two-dimensional array of replicas of the incident signal and reference pulses, yielding an array of holograms, all with horizontal fringes, where the beams cross (Fig. 1).

Additionally, a tilted interference bandpass filter (IBPF) spectrally resolves the diffracted beams based on their horizontal propagation angle (Fig. 2). Indeed, if an IBPF (with effective refractive index μ [27]) has a nominal central wavelength λ_n and is tilted by a horizontal angle β, and if the incident beam has a horizontal angle θ

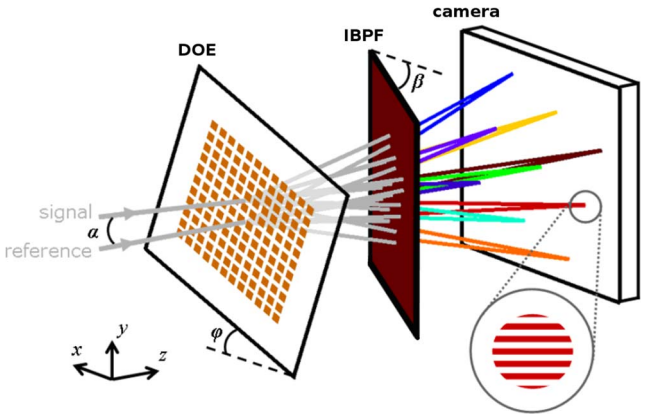

Fig. 1. (Color online) Three-dimensional view of STRIPED FISH. The signal and reference pulses are crossed at a small vertical angle α. The DOE is rotated by an angle φ about the z axis, and the IBPF is rotated by an angle β about the y axis. The inset shows one of the spatial interferograms (digital holograms) captured by the digital camera.

with respect to the optical axis, then the wavelength transmitted by the bandpass filter is given by [28,29]

$$\lambda_t = \lambda_n \left[1 - \frac{(\beta - \theta)^2}{2\mu^2} \right]. \quad (3)$$

This simple relation is valid for angles up to ~20°: For larger angles, the transmitted wavelength begins to depend on polarization. Whenever possible we limit ourselves to the p polarization and to angles less than ~30° to avoid an excessive increase in the filter bandwidth [28]. Small vertical incidence angles on the IBPF have only a second-order contribution to λ_t and are neglected.

Finally, we also orient the DOE so that it is rotated slightly by an angle φ about the optical axis z (see Fig. 1). As a result, the hologram array is also slightly rotated, with the effect that each hologram involves pairs of beams of a different wavelength. The resulting quasi-monochromatic holograms, each at a different color, yield the complete spatial field (intensity and phase) for each

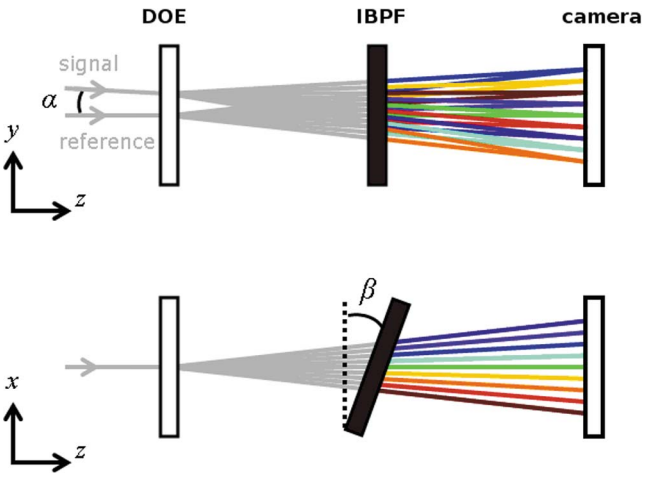

Fig. 2. (Color online) (Top) Side view (y–z plane) showing the signal and reference beams crossing at an angle α. (Bottom) Top view (x–z plane) showing how the frequencies transmitted by the IBPF increase with position x.

color in the pulse and can then be combined to yield the complete spatio-temporal field of the signal pulse, $E(x,y,t)$.

3. RECONSTRUCTION OF THE ELECTRIC FIELD FROM A MEASURED TRACE

To obtain the complex electric field $E(x,y,\omega)$, we apply a variation of the standard reconstruction algorithm used in many interferometric measurements [24]. Figure 3 depicts the process. First, a two-dimensional Fourier transform is applied to the STRIPED FISH trace. When the different holograms are well separated [Fig. 3(a)], the only spatial fringes that are visible are the ones due to the small vertical crossing angle α between the signal and the reference pulses. Therefore, in the Fourier domain [Fig. 3(b)], we expect to obtain one central region corresponding to the noninterferometric terms, and two other regions corresponding to the interferometric terms due to the crossing angle α. We only retain the upper region and inverse Fourier transform it to obtain a complex-valued image [Fig. 3(c)].

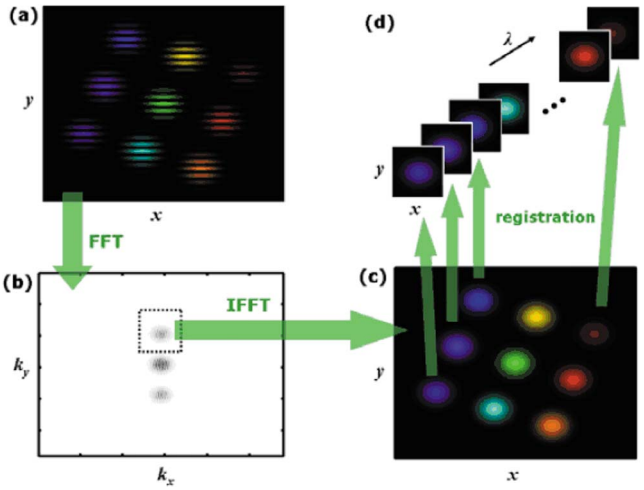

Fig. 3. (Color online) Algorithm used to reconstruct the three-dimensional electric field from a single camera frame. (a) A two-dimensional fast Fourier transform is applied to a simulated STRIPED FISH trace. (b) The interferometric terms are selected in the Fourier plane, and (c) transformed back to the original $x-y$ plane. The resulting image contains both the spatial amplitude and phase, at the expense of a loss of vertical spatial resolution. (d) A registration step is applied to center all the spatial distributions and to assign the calibrated wavelengths in order to obtain the multispectral complex data $E(x,y,\omega)$.

This image contains a collection of spectrally resolved complex electric fields $E(x,y)$ measured at various frequencies ω_k, once we divide by the field of the reference beam field. These electric fields are distributed over the camera frame and need to be centered one by one. We use data from a reference experimental image obtained from a pulse free of spatiotemporal distortions to find the beam center corresponding to each spatial electric field, so that the data can be reorganized into a three-dimensional data cube, $E(x,y,\omega)$. During this registration step, each digital hologram is assigned a frequency ω_k using calibrated data previously obtained by measuring the spectra of the various diffracted beams.

Finally, we apply Eq. (1) to reconstruct the field $E(x,y,t)$ in the time domain. Using diffraction integrals, we can also numerically propagate the electric field through known elements along the z direction if desired to attain the full four-dimensional spatiotemporal field, $E(x,y,z,t)$.

4. EXPERIMENTAL SETUP AND RESULTS

A. Implementation as a Mach–Zehnder Interferometer

As a proof of principle, we set up a STRIPED FISH device as a Mach–Zehnder interferometer [Fig. 4(a)]. A first beam splitter is used to separate a precharacterized incident ultrashort pulse from a mode-locked Ti:sapphire oscillator into a reference and a signal pulse. The pulse to be characterized is then sent into the signal arm before the two pulses are recombined on a second beam splitter. This recombination is quasi collinear: A small vertical angle α is introduced in order to generate horizontal fringes on the digital camera, where both pulses are temporally and spatially overlapped. The temporal overlap is obtained using a delay line that is adjusted to maximize the visibility of the interference fringes.

Between the second beam splitter and the digital camera, we insert the rotated DOE and the tilted IBPF to generate the array of spectrally resolved holograms. The DOE typically consists of an array of 10 μm $\times$ 10 μm re-

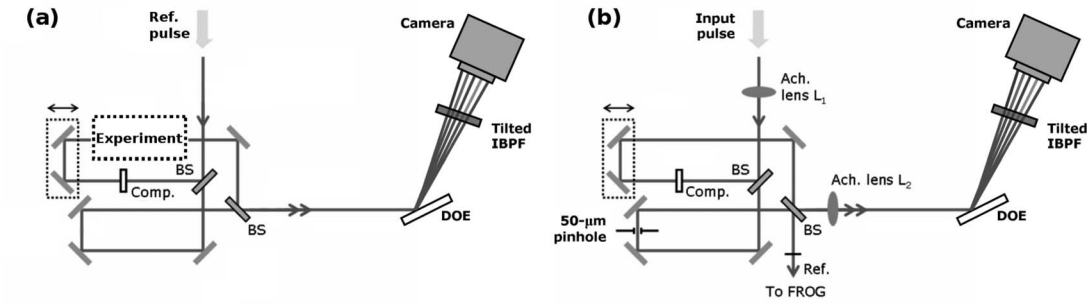

Fig. 4. Mach–Zehnder interferometer used to implement our STRIPED FISH device, drawn in the $x-z$ plane. BS, beam splitter. The optical paths of both arms are matched using the delay stage, and a small vertical angle is introduced between the signal and reference pulses so that horizontal fringes are obtained on the digital camera. (b) Setup used for a fully self-referenced STRIPED FISH. $L_{1,2}$, achromatic doublets arranged as a telescope; Comp, compensating plate. In these top views, the signal and the reference pulses are displaced vertically and overlap on the drawing. The interferometer is dispersion compensated over 200 nm.

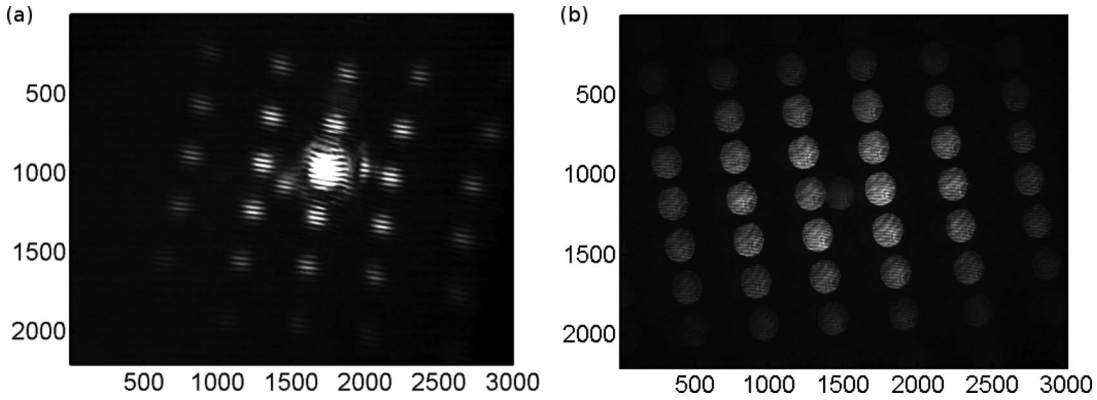

Fig. 5. Typical experimental STRIPED FISH trace (2208×3000 pixels) obtained with a 5 megapixel CMOS camera. The central digital hologram is saturated because of the absence of antireflection coating on the DOE substrate used away from Brewster's angle. (b) Experimental STRIPED FISH trace recorded at Brewster's angle to remove the bright central spot.

flective chrome squares, spaced by 50 μm, on the front surface of a quartz substrate. This optic is used in reflection to avoid dispersion from the substrate. The IBPF (CVI Lasers) has a nominal wavelength of $\lambda_n = 837$ nm and a bandwidth (FWHM) of 3 nm, and we tilt it by an angle of $\beta \approx 20°$ to transmit the pulses centered at 800 nm. We typically generate an array of a least 20 holograms, which are captured by a high-resolution (5 megapixel) complementary metal-oxide semiconductor (CMOS) camera (2208×3000 PixeLINK PL-A781). With this camera, single-shot traces are easily obtained at 800 nm for optical input powers below 100 mW. The wavelength corresponding to each interferogram is calibrated by measuring the local spectrum at that point using a fiber-coupled grating spectrometer (Ocean Optics USB2000).

Figure 5(a) shows a typical STRIPED FISH trace. The central interferogram, corresponding to the undiffracted order of the DOE, is much more intense than the other holograms. This is due to the lack of antireflection coatings on the stock substrate (quartz) of the DOE. When possible, we try to minimize this effect by using signal and reference pulses with horizontal polarizations and that are incident on the DOE at Brewster's angle θ_B (57° for a quartz substrate). An example of a STRIPED FISH trace recorded at Brewster's angle is shown in Fig. 5(b). Compared with Fig. 5(a), the brightness of the central (undiffracted) hologram is greatly reduced, and all the digital holograms can be simultaneously recorded within the dynamic range of a 10 bit digital camera. Note that there is a weak reflection present on the right of the central hologram; it is due to a reflection from the back surface of the DOE substrate and could be easily removed by an index-matching element.

We demonstrate our technique using ultrashort pulses from a mode-locked Ti:sapphire oscillator. The pulses are centered at 800 nm and have approximately 30 nm of bandwidth (FWHM). Because of the high repetition rate (89 MHz) of the laser, our measurement averages over many pulses. With our 1 kHz chirped-pulse amplified system, recording single-shot STRIPED FISH traces was straightforward, however, since submillisecond exposure times are readily obtained by digital cameras (see, for example, Fig. 9 below).

B. Measurement of the Spectral Phase

We first show that STRIPED FISH is sensitive to the spectral phase of the signal pulse by introducing some test phase functions, such as group delay and group-delay dispersion (GDD). This modifies the absolute phase of the fringes of each digital hologram in the experimental STRIPED FISH trace.

Figure 6 depicts the situation. The lower left image corresponds to a STRIPED FISH trace, from which two profiles (gray lines) are extracted. These two profiles are shown using two gray curves on the upper right graph. These profiles are recorded at zero delay between the reference and the signal pulse. A small group delay is then introduced in the signal pulse by slightly translating the delay line of the Mach–Zehnder interferometer. The corresponding STRIPED FISH trace looks similar, except for the absolute position of the spatial fringes (black curves). A careful inspection of two interferograms—labeled (a) and (b)—reveals that there is a relative phase shift caused by the group delay.

This fringe shift is recorded as a function of frequency and corresponds to the spectral phase of the signal pulse (measured with respect to the reference pulse). As expected, a linear spectral phase characteristic of group delay is obtained [Fig. 7(a)].

A similar experiment can be performed by introducing a dispersive window in the signal arm of the interferometer, so that GDD is introduced. The same procedure is repeated, and a characteristic quadratic spectral phase is obtained experimentally [Fig. 7(b)].

C. Measurement of Spatiotemporal Couplings

STRIPED FISH is ideal for measuring spatiotemporal couplings and distortions. As an example, we introduced spatial chirp in the signal beam using a pair of gratings. Figure 8 shows two slices of the reconstructed electric field $E(x,y,t)$ that are obtained by a STRIPED FISH measurement; one slice is obtained at $y=0$ [Fig. 8(a)], and the other at $x=0$ [Fig. 8(b)]. In these plots, the instantaneous wavelength (shown in color) is calculated from the derivative of the temporal phase. Any temporal gradient of the instantaneous wavelength corresponds to temporal chirp, and any spatial gradient is due to spatial chirp. Horizontal spatial chirp is clearly visible in Fig. 8(a).

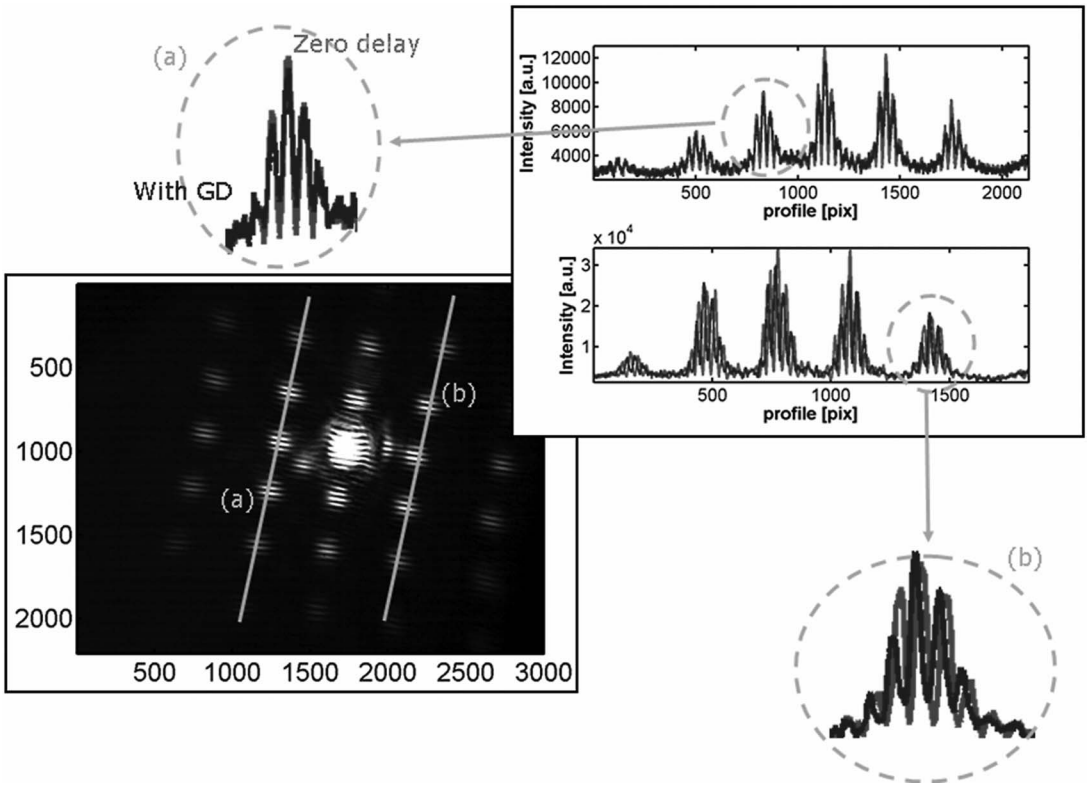

Fig. 6. Encoding of the spectral phase in a STRIPED FISH trace. The lower left image is a STRIPED FISH trace. Two profiles are recorded along the gray lines and graphed on the upper right plot. The insets show the profile of two holograms (a) and (b) recorded at two different wavelengths. Gray curves, zero delay. Black curves, group delay introduced in the signal pulse.

D. Self-Referenced STRIPED FISH

We now introduce a slight modification of the implementation of STRIPED FISH that is fully self-referenced. This device requires only one input pulse, the pulse under test. This pulse is split into two replicas, one of which is spatially filtered to result in a reference pulse (a pulse whose spatial phase is essentially constant). The spectral phase of that reference pulse is therefore free of any spatial dependence and is measured by a FROG device (a Swamp Optics GRENOUILLE) matched to the pulse characteristics [6,30]. This completely characterizes the reference pulse that can then be interfered with the signal pulse in the usual configuration.

Figure 4(b) shows an implementation of a fully self-referenced STRIPED FISH. Additionally, this optical setup is optimized for broadband light. Two achromatic doublets and a 50 μm pinhole form a spatial filter in the reference arm. The lenses are placed in the common path of the interferometer to reduce the effects of dispersion; we also use a 1 mm fused-silica dispersion-compensating plate to cancel the effects of the substrate of the beam splitter. The beam splitter is a half-silvered plate to prevent the higher-order dispersion terms due to multilayer resonance usually present in dielectric beam splitters [31].

The Mach–Zehnder interferometer results in two (pairs

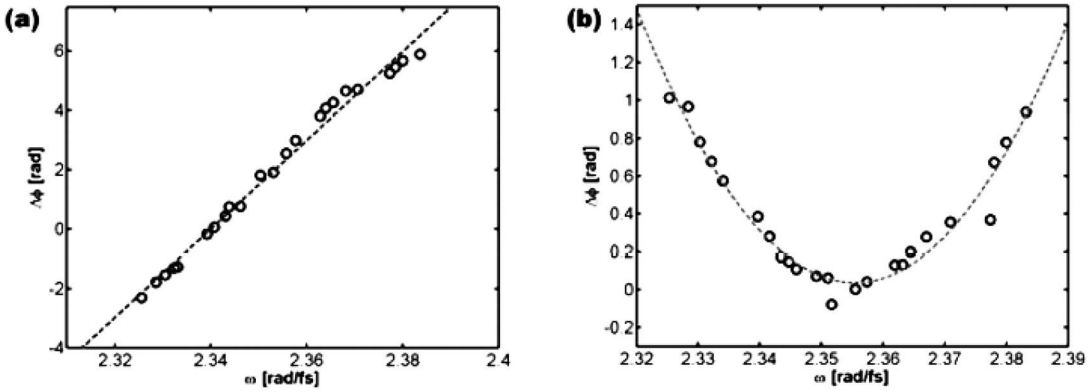

Fig. 7. Fringe shift in each digital hologram as a function of frequency, showing a linear phase due to group delay. Open circles, measurement; dotted line, linear fit. (b) Fringe shift in each digital hologram as a function of frequency, showing a quadratic phase due to group-delay dispersion. Open circles, measurement; dotted curve, quadratic fit.

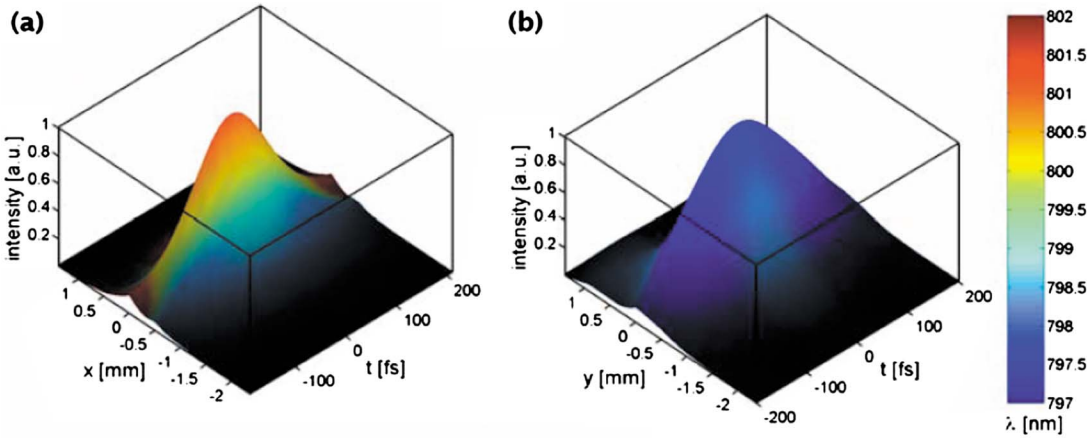

Fig. 8. (Color online) (a) $x-t$ slice of the measured electric field $E(x,y,t)$ of a pulse with spatial chirp. The vertical axis shows the electric field intensity $|E(x,t)|^2$ and the color shows the instantaneous wavelength derived from the phase $\phi(x,t)$. The spatial gradient of color shows the spatial chirp along the x direction. (b) $y-t$ slice of the same measured electric field. No spatial chirp is present along the y direction, as expected.

of) outputs. One pair of output beams (composed of the signal and reference pulses) is crossed at a small vertical angle a and is directed to the DOE. In the other pair of output beams, the signal pulse is blocked and the reference pulse is sent to a FROG device to measure its spectral phase. The FROG device that is used must match the characteristics (bandwidth, duration, complexity) of the pulse to be measured as well as the desired temporal and spectral resolution. Various FROG devices are available [5], and whenever possible we used a compact single-shot second-harmonic-generation (SHG) FROG device [6].

The resulting interferometer is dispersion compensated over a large bandwidth. This is demonstrated by the observation of a STRIPED FISH trace spanning over 200 nm (Fig. 9). This trace was obtained by measuring a very broadband pulse generated by a white-light continuum. An amplified pulse from a chirped-pulse amplifier (~50 μJ, ~200 fs) was focused into a 13 mm fused-silica window. Because of third-order nonlinear effects, the pulse undergoes self-focusing and self-phase modulation in bulk fused silica [32], resulting in very broadband light that appears white to the eye. We did not attempt to reconstruct the full electric field from a white-light continuum, however, because a simultaneous measurement of the temporal and spectral characteristics suggested a spectral complexity [33] that exceeded by far the spectral resolution of STRIPED FISH (see Section 6 for a discussion of the spectral limitations of our device).

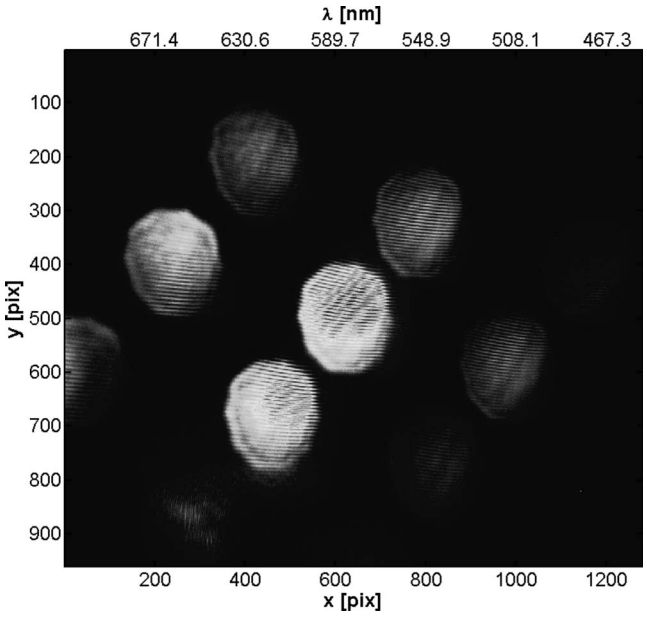

Fig. 9. STRIPED FISH trace recorded with a self-referenced broadband STRIPED FISH obtained with white-light continuum generated in bulk fused silica

5. DESIGN OF THE DIFFRACTIVE OPTICAL ELEMENT

In this section we describe the design parameters and the fabrication process of the DOE. For clarity, its properties (working distance, angular dispersion and resulting spatial chirp) are first described in one dimension and then extended to two dimensions. We call a the width of each square and b the square separation distance.

A. Working Distance

The DOE acts as a coarse reflective grating. Therefore, using an angle of incidence θ_B equal to Brewster's angle, multiple orders m are diffracted in directions θ_m satisfying the grating equation: $\theta_m = \arcsin[m\lambda/b + \sin\theta_B] - \theta_B$.

These angles are defined in the far field of the DOE, i.e., for $z \gg b^2/\lambda_0$. We also require that the diffracted beam pairs do not overlap after a distance z, where the digital camera is placed. For an input beam of size w, this geometrical condition requires that $z > bw/\lambda_0$ (and thus the far-field condition is satisfied since a large number of spatial periods b must be illuminated by the input beam size w). Finally, to avoid self-diffraction effects from this beam, we require that $z \ll w^2/\lambda_0$. To conclude, the working distance of the DOE is given by the following range for z:

$$\frac{bw}{\lambda_0} \ll z \ll \frac{w^2}{\lambda_0}. \tag{4}$$

The working distance given by Eq. (4) also holds for the case of a two-dimensional DOE. For a typical design at

800 nm ($b=50$ μm, with $b/a=5$), the working distance is given approximately by 20 cm$\ll z \ll$1000 cm.

B. Diffracted-Order Efficiency

The diffraction efficiency of the various orders of the DOE depends on the shape of one individual spatial period. In the far field, the efficiency (in intensity) in one dimension is given by the modulus squared of the Fourier transform of Rect(x/a), i.e., sinc$^2(ak_x/2)$. Since the orders are spaced by $2p/b$ in k_x space, the intensity of order m is sinc$^2(mpa/b)$, which falls to ~40% of the maximum for $m \simeq b/(2a)$. Therefore, the number of orders that are diffracted with more than 40% efficiency in one dimension is approximately given by b/a. In two dimensions, this number becomes $(b/a)^2$. Larger ratios result in an increase in the number of useful diffracted orders but reduce the overall efficiency of the DOE in the same proportion. Thus, there is a trade-off between the number of holograms on a STRIPED FISH trace, and the device efficiency, or equivalently, between the spectral resolution and the throughput.

C. Angular Dispersion Introduced by the DOE

The DOE necessarily introduces angular dispersion in the orders $m \neq 0$. At first sight, this effect might seem problematic for two reasons: It might affect the angle-tuning properties of the IBPF, and it may result in spatial chirp in the digital holograms recorded by the digital camera. In this section, we show that both distortions are negligible for typical design parameters.

We first consider the angular dispersion of the diffracted beams. Typically, $b \gg \lambda$, and the angular dispersion is $(d\theta/d\lambda)_{DOE} \simeq m/b$. This parameter must be compared with the differential form of the angle-tuning equation [Eq. (3)]:

$$\left(\frac{d\theta}{d\lambda}\right)_{IBPF} \simeq \frac{\mu^2}{\lambda_n \beta}. \tag{5}$$

If the IBPF is tilted by an angle β such that it passes the central wavelength of the pulse (λ_0) for $m=0$, then Eq. (5) reduces to

$$\left(\frac{d\theta}{d\lambda}\right)_{IBPF} \simeq \frac{\mu}{\sqrt{2\lambda_n(\lambda_n-\lambda_0)}}. \tag{6}$$

Because μ and m are of order unity and $b \gg \lambda_0 > \lambda_n - \lambda_0$, we conclude that $(d\theta/d\lambda)_{DOE} \ll (d\theta/d\lambda)_{IBPF}$, i.e., the effects of angular dispersion of the DOE can be neglected compared with the angle dependence of the wavelength passed by the IBPF.

The second concern is the residual spatial chirp present in each hologram recorded by the digital camera. Spatial chirp increases with the distance z from the DOE and, at the position where the diffracted beams start to separate, is given by

$$\rho_{x\lambda} \simeq \sqrt{2m\frac{\Delta\lambda_F}{\lambda_0}}. \tag{7}$$

Here, $\Delta\lambda_F$ is the bandwidth transmitted by the IBPF and we quote spatial chirp values in terms of a normalized correlation parameter $\rho_{x\lambda}$ that varies between −1 and +1 (see [34]). Since the largest order m that is efficiently diffracted is $\sim b/(2a)$, this gives a maximum value for spatial chirp of

$$\rho_{x\lambda} \simeq \sqrt{\frac{b}{a}\frac{\Delta\lambda_F}{\lambda_0}}. \tag{8}$$

With b/a ratios in the range of 5–10, we need $\Delta\lambda_F < \lambda_0/100$ to keep $\rho_{x\lambda}$ below 0.30, an acceptable value in most situations [34]. At 800 nm, this requires a bandpass filter with a bandwidth below 8 nm, which is easily satisfied.

D. Fabrication

Because an optimal DOE requires careful design, it is unlikely that stock two-dimensional diffraction gratings (e.g., Max Levy FA079, Thorlabs BPD254-FS) satisfy all the requirements described above. To allow for more flexibility, we usually design our own DOE. This optical element closely resembles photomasks (also called reticles) that are used in the microelectronics industry [35]. As a fortunate consequence, custom photomasks are inexpensive to fabricate. They typically consist of a transparent substrate (soda lime or quartz) on which a layer (iron oxide or chromium) opaque to UV light is patterned by electron-beam lithography. For our application, we choose chromium, a coating opaque in the UV (the spectral region normally used with photomasks) but partially reflective in the near IR. The mask is designed using standard CAD tools before being converted into the appropriate format for a pattern generator machine. Feature sizes of the order of a few micrometers were easily obtained during the fabrication of such masks both on site (Georgia Tech Micro-electronics Research Center) and at an external company (Photo Sciences Inc.).

6. CHARACTERISTICS AND LIMITATIONS OF STRIPED FISH

A. Spectral Range

Interference filters can be used with incidence angles up to ~30°. This sets a limit to the spectral range they can cover, or equivalently, to the bandwidth they can support. For a Gaussian spectrum with FWHM $\Delta\lambda$, the range of wavelengths with spectral density above 6% (respectively, 0.5%) of the peak is twice (respectively, three times) the FHWM. To simplify the following equations we define $\Delta\lambda_{range}=2\Delta\lambda$. For a typical value of $\mu=1.45$, an angle $\beta-\theta$ of 30° gives in Eq. (3) a value of $(\lambda_n-\lambda_0)\simeq 0.065\lambda_n$. Since $(\lambda_n-\lambda_0)\simeq\Delta\lambda_{range}/2$, we have $\Delta\lambda < 0.065\lambda_0$. At 800 nm, this results in a maximum bandwidth of $\Delta\lambda < 50$ nm. For larger pulse bandwidths it is preferable to use a filter whose passed wavelength depends on the transverse position x (e.g., Schott VERIL VIS-60).

Although the IBPF can support a maximum spectral range of $2\Delta\lambda = 2\times 0.065\lambda_0$, the effective spectral range that is covered depends on the parameters of the DOE. Assuming that $b > a \gg \lambda$, the range of diffracted angles is given by λ/a. According to Eq. (7), this results in a spectral range of

$$\Delta\lambda_{range} = \frac{\lambda_0}{\mu a}\sqrt{2\lambda_n(\lambda_n - \lambda_0)}. \quad (9)$$

B. Spectral Resolution

Now let us consider the second condition regarding the desired spectral resolution $\delta\lambda$ of the system. We assume that the bandwidth of the interference filter is smaller than $\delta\lambda$, even under an oblique incidence. In that case, $\delta\lambda$ is simply given by the spectral range divided by the number of diffracted beams. In the two-dimensional case, we obtain $d\lambda/\Delta\lambda \simeq 2a^2/b^2$ or

$$\delta\lambda \simeq \frac{2\lambda_0 a}{\mu b^2}\sqrt{2\lambda_n(\lambda_n - \lambda_0)}. \quad (10)$$

Note that as the spectral resolution is improved, for example, by increasing the number of captured holograms, it might reach the bandwidth of the spectral filter, which will then become the limiting factor.

C. Spatial Resolution

The spatial resolution of STRIPED FISH is limited by two effects: the spatial period b of the DOE and the size of the filtering window in the Fourier domain used in the reconstruction algorithm. In practice, this last effect is the limiting factor and typically results in a spatial resolution slightly worse than the spatial period b. A camera with a larger imaging sensor and smaller pixel size will therefore result in an improvement in the number of holograms that can be captured and in a better spatial resolution that will eventually be limited to b.

D. Spatiotemporal Complexity

Finally, we note that it is possible to quantify the overall performance of STRIPED FISH with regard to the spatiotemporal complexity it can support. Indeed, the maximum time–bandwidth product (TBP) that we can hope to measure is roughly equal to the number of holograms that are captured. Similarly, the maximum space–bandwidth product (SBP) is approximately equal to the number of spatial points obtained by the reconstruction algorithm. As a result, the amount of information (number of independent data points) and therefore the maximum pulse complexity that STRIPED FISH can measure is estimated by introducing the space–time–bandwidth product TBP$\times$SBP, which is usually of the order of 10^5, approximately one hundredth to one tenth the number of camera pixels.

7. CONCLUSIONS

Wavelength-multiplexed digital holography allows us for the first time to our knowledge to completely characterize (i.e., in intensity and phase and as a function of three dimensions x, y, and t) the electric field of a femtosecond laser pulse using a configuration compatible with single-shot detection. This method has been experimentally implemented using a simple device (STRIPED FISH) based on only a few key elements: a diffractive beam splitter, a spectral filter, and a high-resolution digital camera. We demonstrated the measurement of spatiotemporal distortions, a chief preoccupation in amplified systems.

Our current implementation, however, leaves room for improvement. One drawback, for instance, is the overall low efficiency of the DOE, in particular when a large number of diffracted beams is sought (i.e., $b/a \gg 1$). This poses a problem for the single-shot measurement of unamplified pulses. One potential solution is to use a DOE with phase (rather than amplitude) modulation; another approach is the recycling of the strong undiffracted order that could be used as a reference pulse after appropriate spatial filtering and zero-delay synchronization (a similar idea has been demonstrated in the context of film holograms [36]).

Other areas that could benefit from an improved design are the spectral and spatial resolutions of the device. The spectral resolution is presently limited by the bandwidth of the stock interference filter. Custom dielectric components or a high-finesse etalon should be able to considerably improve the spectral resolution of the device. The spatial resolution currently depends on the number of pixels in the digital camera. Although we used a fairly high pixel-count system (>5 megapixels), the resolution of these systems is ever increasing. Sensors with tens of megapixels are now commonly available. With a higher pixel count, it can be expected that the spatial resolution of a STRIPED FISH device and its maximum measurable pulse space–time–bandwidth product can be substantially increased.

ACKNOWLEDGMENTS

We gratefully acknowledge support from the National Science Foundation (grant ECS-0200223), the Georgia Research Alliance, and Georgia Tech.

REFERENCES

1. C.-C. Chang, H. P. Sardesai, and A. M. Weiner, "Dispersion-free fiber transmission for femtosecond pulses by use of a dispersion-compensating fiber and programmable pulse shaper," Opt. Lett. **23**, 283–285 (1998).
2. E. Zeek, R. Bartels, M. M. Murnane, H. C. Kapteyn, S. Backus, and G. Vdovin, "Adaptive pulse compression for transform-limited 15 fs high-energy pulse generation," Opt. Lett. **25**, 587–589 (2000).
3. F. Druon, G. Chériaux, J. Faure, J. Nees, M. Nantel, A. Maksimchuk, G. Mourou, J.-C. Chanteloup, and G. Vdovin, "Wave-front correction of femtosecond terawatt lasers by deformable mirrors," Opt. Lett. **23**, 1043–1045 (1998).
4. J.-C. M. Diels, J. J. Fontaine, I. C. McMichael, and F. Simoni, "Control and measurement of ultrashort pulse shapes (in amplitude and phase) with femtosecond accuracy," Appl. Opt. **24**, 1270–1282 (1985).
5. R. Trebino, K. W. DeLong, D. N. Fittinghoff, J. N. Sweetser, M. A. Krumbuegel, and D. J. Kane, "Measuring ultrashort laser pulses in the time-frequency domain using frequency-resolved optical gating," Rev. Sci. Instrum. **38**, 3277–3295 (1997).
6. P. O'Shea, M. Kimmel, X. Gu, and R. Trebino, "Highly simplified device for ultrashort measurement," Opt. Lett. **26**, 932–934 (2001).
7. B. C. Platt and R. Shack, "History and principles of Shack–Hartmann wavefront sensing," J. Cataract Refractive Surg. **17**, S573–S577 (2001).

8. J. Liang, B. Grimm, S. Goelz, and J. F. Bille, "Objective measurement of wave aberrations of the human eye with the use of a Hartmann–Shack sensor," J. Opt. Soc. Am. A **11**, 1949–1957 (1994).
9. R. G. Lane and M. Tallon, "Wave-front reconstruction using a Shack–Hartmann sensor," Appl. Opt. **31**, 6902–6908 (1992).
10. E. Leith, C. Chen, Y. Chen, D. Dilworth, J. Lopez, J. Rudd, P. C. Sun, J. Valdmanis, and G. Vossler, "Imaging through scattering media with holography," J. Opt. Soc. Am. A **9**, 1148–1153 (1992).
11. S. Grilli, P. Ferraro, S. De Nicola, A. Finizo, G. Pierattini, and R. Meucci, "Whole optical wavefield reconstruction by digital holography," Opt. Express **9**, 294–302 (2001).
12. S. Lai, B. King, and M. A. Neifeld, "Wave front reconstruction by means of phase-shifting digital in-line holography," Opt. Commun. **173**, 155–160 (2000).
13. S. Akturk, X. Gu, P. Gabolde, and R. Trebino, "The general theory of first-order spatio-temporal distortions of Gaussian pulses and beams," Opt. Express **13**, 8642–8661 (2005).
14. S. Akturk, X. Gu, E. Zeek, and R. Trebino, "Pulse-front tilt caused by spatial and temporal chirp," Opt. Express **12**, 4399–4410 (2004).
15. Z. Bor, "Distortion of femtosecond laser pulses in lenses," Opt. Lett. **14**, 119–121 (1989).
16. Z. Bor and Z. L. Horvath, "Distortion of femtosecond pulses in lenses. Wave optical description," Opt. Commun. **94**, 249–258 (1992).
17. Z. Bor, B. Racz, G. Szabo, M. Hilbert, and H. A. Hazim, "Femtosecond pulse front tilt caused by angular dispersion," Opt. Eng. **32**, 2501–2504 (1993).
18. M. Kempe and W. Rudolph, "Impact of chromatic and spherical aberration on the focusing of ultrashort light pulses by lenses," Opt. Lett. **18**, 137–139 (1993).
19. J. Néauport, N. Blanchot, C. Rouyer, and C. Sauteret, "Chromatism compensation of the PETAL multipetawatt high-energy laser," Appl. Opt. **46**, 1568–1574 (2007).
20. G. Pretzler, A. Kasper, and K. J. Witte, "Angular chirp and tilted light pulses in CPA lasers," Appl. Phys. B **70**, 1–9 (2000).
21. T. Tanabe, H. Tanabe, Y. Teramura, and F. Kannari, "Spatiotemporal measurements based on spatial spectral interferometry for ultrashort optical pulses shaped by a Fourier pulse shaper," J. Opt. Soc. Am. B **19**, 2795–2802 (2002).
22. K. Varju, A. P. Kovacs, G. Kurdi, and K. Osvay, "High-precision measurement of angular dispersion in a CPA laser," Appl. Phys. B **74**, 259–263 (2002).
23. P. Gabolde and R. Trebino, "Self-referenced measurement of the complete electric field of ultrashort pulses," Opt. Express **12**, 4423–4428 (2004).
24. M. Takeda, H. Ina, and S. Kobayashi, "Fourier-transform method of fringe-pattern analysis for computer-based topography and interferometry," J. Opt. Soc. Am. **72**, 156–160 (1982).
25. P. Gabolde and R. Trebino, "Single-shot measurement of the full spatio-temporal field of ultrashort pulses with multi-spectral digital holography," Opt. Express **14**, 11460–11467 (2006).
26. Z. Liu, M. Centurion, G. Panotopoulos, J. Hong, and D. Psaltis, "Holographic recording of fast events on a CCD camera," Opt. Lett. **27**, 22–24 (2002).
27. P. H. Lissberger, "Properties of all-dielectric interference filters. I. A new method of calculation," J. Opt. Soc. Am. **49**, 121–125 (1959).
28. M. Bass, *Handbook of Optics*, 2nd ed. (Optical Society of America, 1995), pp. 4289–4290.
29. P. H. Lissberger and W. L. Wilcock, "Properties of all-dielectric interference filters. II. Filters in parallel beams of light incident obliquely and in convergent beams," J. Opt. Soc. Am. **29**, 126–130 (1959).
30. P. O'Shea, S. Akturk, M. Kimmel, and R. Trebino, "Practical issues in ultra-short-pulse measurements with 'GRENOUILLE'," Appl. Phys. B **79**, 683–691 (2004).
31. K. Naganuma, K. Mogi, and H. Yamada, "Group-delay measurement using the Fourier transform of an interferometric cross correlation generated by white light," Opt. Lett. **15**, 393–395 (1990).
32. A. Brodeur and S. L. Chin, "Ultrafast white-light continuum generation and self-focusing in transparent condensed media," J. Opt. Soc. Am. B **16**, 637–649 (1999).
33. D. Lee, P. Gabolde, and R. Trebino, "Toward single-shot measurement of continuum," J. Opt. Soc. Am. B, doc. ID 89269 (posted 4 March 2008, in press).
34. P. Gabolde, D. Lee, S. Akturk, and R. Trebino, "Describing first-order spatio-temporal distortions in ultrashort pulses using normalized parameters," Opt. Express **15**, 242–251 (2007).
35. J. P. Uyemura, *Introduction to VLSI Circuits and Systems* (Wiley, 2001).
36. C. Bhan, L. Mainali, D. Mohan, and A. K. Gupta, "Recycling of undiffracted laser light for reconstruction of holograms," Opt. Lasers Eng. **35**, 355–360 (2001).